2140–2151 *Nucleic Acids Research, 2012, Vol. 40, No. 5* *Published online 3 November 2011*
doi:10.1093/nar/gkr894

Characterization of the kinetic and thermodynamic landscape of RNA folding using a novel application of isothermal titration calorimetry

Kirk A. Vander Meulen* and Samuel E. Butcher*

Department of Biochemistry, University of Wisconsin-Madison, 433 Babcock Dr Madison, WI 53706, USA

Received August 22, 2011; Revised September 29, 2011; Accepted October 3, 2011

ABSTRACT

A novel isothermal titration calorimetry (ITC) method was applied to investigate RNA helical packing driven by the GAAA tetraloop–receptor interaction in magnesium and potassium solutions. Both the kinetics and thermodynamics were obtained in individual ITC experiments, and analysis of the kinetic data over a range of temperatures provided Arrhenius activation energies ($\Delta H^{\ddagger}$) and Eyring transition state entropies ($\Delta S^{\ddagger}$). The resulting rich dataset reveals strongly contrasting kinetic and thermodynamic profiles for this RNA folding system when stabilized by potassium versus magnesium. In potassium, association is highly exothermic ($\Delta H_{25^{\circ}C} = -41.6 \pm 1.2$ kcal/mol in 150 mM KCl) and the transition state is enthalpically barrierless ($\Delta H^{\ddagger} = -0.6 \pm 0.5$). These parameters are sigificantly positively shifted in magnesium ($\Delta H_{25^{\circ}C} = -20.5 \pm 2.1$ kcal/mol, $\Delta H^{\ddagger} = 7.3 \pm 2.2$ kcal/mol in 0.5 mM $MgCl_2$). Mixed salt solutions approximating physiological conditions exhibit an intermediate thermodynamic character. The cation-dependent thermodynamic landscape may reflect either a salt-dependent unbound receptor conformation, or alternatively and more generally, it may reflect a small per-cation enthalpic penalty associated with folding-coupled magnesium uptake.

INTRODUCTION

Proper tertiary folding of RNA is crucial to its array of enzymatic and regulatory functions (1). Due to the significant increase in anionic charge density and structure-dependent apposition of phosphate oxygens that accompany RNA tertiary folding, metal ions play a significant and nuanced role in the folding equilibrium. Beginning with the seminal series of tRNA folding studies (2–8), the highly stabilizing role of the divalent cation magnesium (Mg^{2+}) has been an experimental focal point. Misra and Draper (9) demonstrated that Mg^{2+} can confer this stability to folded tRNA entirely through diffuse (hydrated) ion accumulation, consistent with the fact that tRNA can fold in magnesium salt or monovalent salt alone (2). For some other RNA structures, magnesium is directly coordinated and essential for folding (10,11); in principle, intermediate hydration states are also possible although the prevalence and thermodynamic stability afforded by these types of ions is not well understood. Such molecular considerations may underlie the systematic underestimation of magnesium accumulation by Poisson–Boltzmann theory (12). As theoretical work continues in this area (13–15), additional complementary experiments studying this crucial component of RNA stability are also necessary.

In addition to the nature of association (11) and the change in charge density accompanying RNA folding (16), the quantitative role of magnesium depends strongly on the concentration and identity of other metal ions (17). This is an important consideration given *in vivo* free potassium (K^{+}) concentrations near 150 mM. The *Tetrahymena thermophila* Group I self-splicing intron provides an excellent case study. For the P4–P6 domain of this ribozyme, the GAAA tetraloop–receptor tertiary interaction can form in solutions containing either $MgCl_2$ or monovalent salt (NaCl) alone (18–20), but formation of the A-rich bulge tertiary contact requires magnesium (20). While the uptake of Mg^{2+} and Na^{+} is tied to tertiary folding, and addition of either improves folding stability via a reduced entropic penalty, in some concentration regimes when both ions are present they act competitively (21). Interestingly, salt-dependent differences in RNA folding kinetics have also been observed. For example, at salt concentrations that elicit similar overall folding stabilities, intron folding is faster when driven by monovalent cations than when driven by a multivalent cation such as magnesium (22–24). The underlying

*To whom correspondence should be addressed. Tel: +608 213 3952; Email: kvandermeulen@biochem.wisc.edu
Correspondence may also be addressed to Samuel E. Butcher. Tel: +608 263 3890; Fax: +608 262 3453; Email: butcher@biochem.wisc.edu

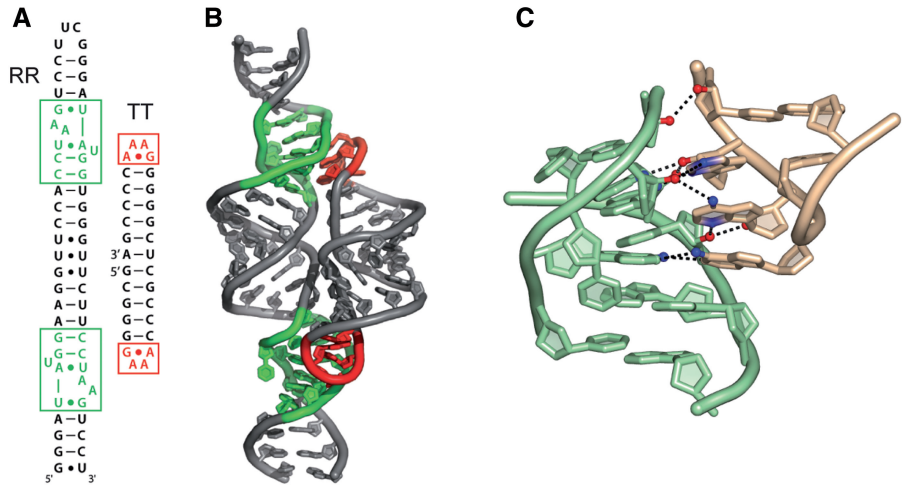

Figure 1. Structure of the TT–RR system. Red/salmon: tetraloop; green/mint: receptor. (**A**) Secondary structure of dual receptor (RR) and dual tetraloop (TT) constructs employed in this study. (**B**) Cartoon model of TT–RR complex. (**C**) Close-up view of tetraloop–receptor interaction, structurally stabilized by stacking of the tetraloop 5′ adenine on the 3′ adenine of the receptor AA platform, in addition to 10 intermolecular hydrogen bonds (PDB code 1HR2).

thermodynamic composition of these findings is not yet understood.

The ubiquitous GAAA tetraloop receptor mediates helical packing (25) in Groups I and II self-splicing introns (26–28) and RNase P (29,30). In this work we examine a bimolecular helical packing event driven by this interaction (Figure 1) (31), in solutions containing either one of the physiologically dominant cations, K^+ or Mg^{2+}. This domain separation strategy has proven successful in determining RNA folding principles (32–35) and allows access to the rich thermodynamic information provided by calorimetry. The approach involves two helical RNA molecules, one containing two tetraloop receptor motifs phased by one helical turn (termed RR) and another containing two cognate GAAA tetraloops (TT). The helices therefore assemble in parallel into a well-defined structure mediated solely by the tetraloop–receptor interaction (Figure 1), as demonstrated by our previous thermodynamic investigation (32) and excellent agreement with single molecule fluorescence resonance energy transfer (FRET) studies of tethered tetraloop receptors (36). We have also solved the nuclear magnetic resonance structure of this interaction, which within experimental error is superimposable with previous crystal structures (18,28,37).

Mg^{2+} accumulation in the tetraloop–receptor contact is entirely or largely diffuse (10,11) in character (18,28). Thus a direct comparison of folding in $MgCl_2$ and KCl can potentially uncover core energetic differences in Mg^{2+} and K^+ accumulation. Here, by application of a novel titration calorimetry approach, we characterize the thermodynamic and kinetic landscape of tetraloop–receptor mediated helical packing interaction when stabilized by either K^+ or Mg^{2+}. We find that the thermodynamic and kinetic profiles for tetraloop–receptor association are indeed significantly dependent on the identity of the cation, such that the transition state enthalpy barrier is on average 9 kcal/mol larger and the overall binding enthalpy is 19 kcal/mol less exothermic in $MgCl_2$ relative to the values in KCl.

MATERIALS AND METHODS

Preparative methods

TT and RR RNA were prepared by *in vitro* transcription and quantitated as described previously (32,37). All samples were prepared for calorimetry by extensive dialysis. Magnesium solutions contained 20 mM 4-(2-hydroxyethyl)-1-piperazineethanesulfonic acid (HEPES) and $MgCl_2$ at the stated concentration; potassium solutions contained 20 mM HEPES, 1 mM ethylenediaminetetraacetic acid, and the stated KCl concentration. Both solutions were titrated to pH 7.0 at room temperature before dialysis.

ITC thermodynamics analysis

Binding data were analyzed as described previously. A small fraction of TT misfolds during preparation (32). This is accounted for using a TT 'activity' term in the binding data and in $[RNA]_{free}$ determinations used in kinetics analysis below; the fraction of active TT in the experiments herein ranged from 0.75–1.0. Error estimates throughout this work reflect a potential uncertainty in the active TT concentration of ±10%. As per standard protocol, the first data point is removed from analysis due to syringe dead volume complications.

ITC kinetics analysis

Following baseline subtraction and deconvolution [(38), Supplementary Data], an injection power trace reflects the real-time derivative of the negative of heat evolution within the calorimeter cell, and subsequent integration results in the negative of the corresponding heat evolution as a function of time (Q_{ev}). Q_{ev} for each injection is approximately described as the time-dependent

concentration of new complex formed [C*(t)] scaled by the binding enthalpy and the sample cell volume ($V_0 = 1.42$ ml).

$$Q_{ev}(t) = -\Delta H V_0 C^*(t) \quad (1)$$

The equilibrium involves three species, so knowledge of the total TT and RR concentrations reduces the description of all solution concentrations to a single degree of freedom, which can be defined in terms of the displacement from equilibrium, λ. Here we define λ as the difference between the equilibrium concentration $[C]_{eq}$ and the current concentration [C]. The reaction rate can then be written

$$\frac{\partial[C]}{\partial t} = -\frac{\partial\lambda}{\partial t} = k_{on}([TT]_{eq}+\lambda)([RR]_{eq}+\lambda) - k_{off}([C]_{eq} - \lambda) \quad (2)$$

Assuming only that $K_d = k_{off}/k_{on}$, Equation (3) is the resulting most general expression for λ, which cannot be expressed analytically.

$$\ln\left(\frac{\lambda_{t=0}}{\lambda}\bullet\frac{[TT]_{eq}+[RR]_{eq}+K_d+\lambda}{[TT]_{eq}+[RR]_{eq}+K_d+\lambda_{t=0}}\right) = -\left([TT]_{eq}+[RR]_{eq}+K_d\right)k_{on}t \quad (3)$$

Here $\lambda_{t=0}$ is the displacement from equilibrium following addition of RNA. More precisely in the case of an ITC experiment, it is the displacement at a theoretical time point following the injection period but preceding formation of any new complexes. $\lambda_{t=0}$ also reflects concentration changes caused by the addition of titrant and by the dilution of all species due to the injection volume ($\lambda_{t=0} = [C]_{eq} - [C]_{t=0+}$, where $[C]_{t=0+}$ is the starting [C] after accounting for the injection-caused dilution). Equation (3) shows that in the most general case, determination of $\lambda(t)$ requires prior knowledge of k_{on}, K_a (i.e. k_{off}), and the total starting concentrations. In our application, the latter two terms are known: the total RNA concentrations are defined for each injection by the experimental setup, and K_a is obtained directly in the same experiment or through an extrapolation from higher temperature according to the van't Hoff equation.

Because λ cannot be determined analytically, its numerical solution from Equation (3) is wrapped within a least squares procedure for determining k_{on}. The predicted heat evolution function is given by

$$Q_{ev} = -\Delta H V_0(\lambda_{t=0} - \lambda) \quad (4)$$

where $\lambda_{t=0}$ is a known quantity defined by the K_a and the RNA concentrations and λ is a function of k_{on}. Data were fit to a time regime starting at the minimum in the raw power trace (to exclude the injection period from analysis), and the final fitted time point never exceeded 10 times a prior-estimated half-time (to avoid overweighting the baseline). Only injections from the first half of a titration were analyzed because signal-to-noise decreases significantly for subsequent injections.

Kinetic data fitting may be performed by integrating the post-deconvolution power trace to obtain Q_{ev} for least squares minimization with target Equation (4).

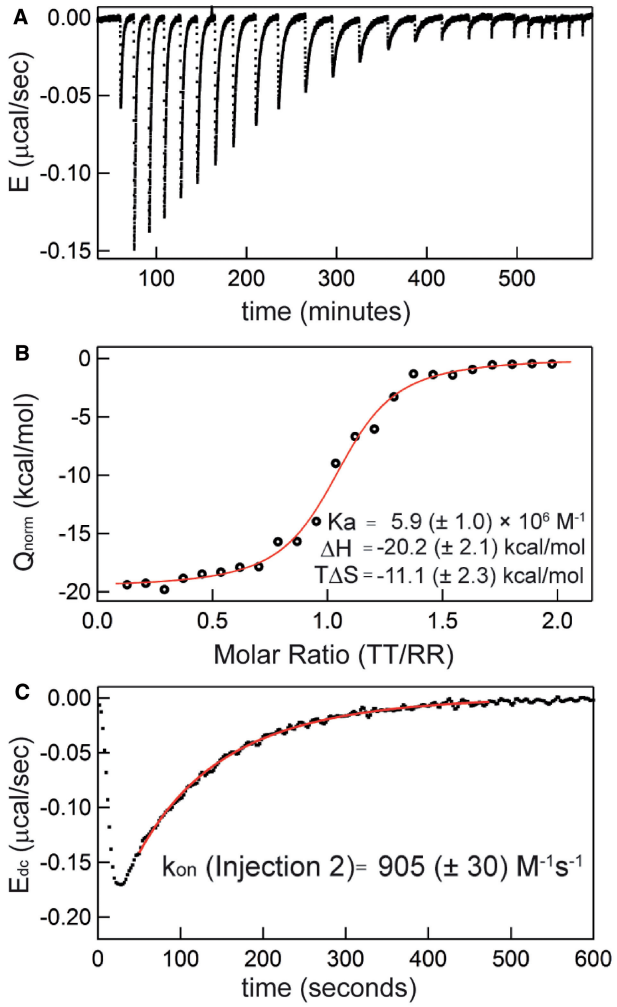

Figure 2. Extraction of both thermodynamic and kinetic parameters from a single binding titration. Forward titration with titrant [TT] = 229 µM, starting cell [RR] = 10 µM, using 5 µL injections, at 20°C in 0.5 mM $MgCl_2$ solution. (**A**) Raw power trace following baseline subtraction to present excess power [$E = (\partial Q/\partial t)$]. (**B**) Binding curve following integration of each peak to plot the concentration-normalized heat evolved (Q_{norm}) against the current molar ratio. Best fit parameters for the displayed dataset are listed. (**C**) Injection Peak 2 following deconvolution (E_{dc}); best-fit curve and resulting k_{on} value for the peak using fit methodology as described in 'Materials and Methods' section are provided.

Alternatively, Equations (3) and (4) can be differentiated for comparison with the deconvolved power trace (E_{dc}). We implemented the latter approach here (Figure 2).

All experiments were performed on a GE Healthcare Microcal VP-ITC, using a feedback setting of 'high', a stirring rate of 307 rpm, and an injection rate of 0.5 µL/sec. The feedback setting was chosen to maximize the instrument response rate constant; the latter two settings have little effect on the instrument response time. The slow kinetics are also not complicated by any RNA dilution effect (Supplementary Figure S1).

Error analysis

A weighted average k_{on} was determined for each titration experiment from the population of individual injection

measurements. The underlying error in these individual determinations is a combination of random noise, baseline drift and uncertainty in the instrumental rate constant (k_{ITC}). The true uncertainty also contains contributions from uncertainty in K_a and in the RNA concentrations. All of these error sources were incorporated into both k_{on} and k_{off} measurements through error propagation as described in Supplementary Data. Higher order analysis of data, such as measurement of slope values to determine $\Delta H^{\ddagger}$, used a 'nested' bootstrap approach to properly estimate error (Supplementary Data). All data processing and analysis routines were implemented and performed using the high-level programming language in Igor Pro 6.

RESULTS

Extraction of thermodynamic and kinetic parameters from a single ITC experiment

Figure 2 shows a typical ITC experiment in which both thermodynamic and kinetic measurements are obtained. The experiment depicted is a titration in which TT RNA is serially injected into a cell initially containing 10 μM RR. The data demonstrate exothermic binding as a series of TT injection-induced negative deflections in the compensatory power trace followed by a slow decay back to the relative baseline value of 0.0 μW (Figure 2A). Integration of each peak yields the heat evolved by binding, which is plotted against the corresponding molar ratio ([TT]/[RR]) for each injection to generate an ITC binding isotherm (Figure 2B). The binding enthalpy (ΔH) and binding constant (K_a) are determined through least squares fits to these binding data ('Materials and Methods' section).

A typical titration microcalorimeter power compensation trace can be viewed as the convolution of a binding-generated 'impulse' heat evolution function with the calorimeter 'response' function. Using a Laplace Transform approach with an instrumental time constant of 12.5 s, the heat evolution function is recovered (deconvolved) for each injection [(38), Supplementary Data]. A representative deconvolved peak and the associated least squares-minimized kinetics curve are displayed in Figure 2C. This fitting procedure in general requires knowledge of the equilibrium RNA concentrations ('Materials and Methods' section); in Figure 2, these values were obtained from the total RNA concentrations and the measured binding constant (Figure 2B). Below, the thermodynamic results from this study are analyzed first, then the corresponding kinetic data are considered.

Comparison of the thermodynamics of tetraloop–receptor association in KCl and $MgCl_2$

Analysis of TT–RR binding data reveals strikingly different thermodynamic profiles for this helical packing event in $MgCl_2$ and KCl solutions (Figure 3). Representative experiments performed at 20°C in either 0.5 mM $MgCl_2$ or 150 mM KCl demonstrate that, while binding is enthalpy-driven in both salts, in KCl it is significantly more exothermic (for these conditions, on average $\Delta\Delta H = -21.7$ (± 3.7) kcal/mol) and less favorable entropically ($\Delta(-T\Delta S) = +22.4$ (± 3.8) kcal/mol) (Figure 3A). The differences in these terms represent contributions to ΔG that are nearly three times greater than the overall stabilities.

To more fully describe the folding landscapes in $MgCl_2$ and KCl, we performed calorimetry experiments in a range of salt concentrations and temperatures (Tables 1 and 2). In aggregate the thermodynamic data are highly self-consistent. K_a increases as a function of added $MgCl_2$ or KCl, and it decreases with increasing temperature.

Figure 3B plots the thermodynamics for TT–RR binding across the full set of examined salt conditions at a common temperature (25°C); the values are also listed in Table 3. The significant discrepancy in $MgCl_2$ and KCl thermodynamic profiles persists across the examined salt concentrations. ΔH_{25C} is bounded by −24.6 and −20.5 kcal/mol in the ensemble of $MgCl_2$ solutions; in KCl the minimum and maximum values are −41.6 and −34.0, respectively. Contrastingly, $T\Delta S_{25C}$ ranges from −16.5 to −10.7 kcal/mol in $MgCl_2$ while it is much more unfavorable in KCl solutions, ranging from −27.4 to −33.8 kcal/mol.

These 25°C thermodynamic quantities are maximum likelihood (i.e. 'optimized') values from the full set of measurements across a range of experimental temperatures. ΔH_{25C} values were calculated for each salt condition from linear fits of individual ΔH measurements plotted against the experimental temperature. The average slopes from these measurements are also given in Table 3 as the heat capacity change ($\Delta C_p = \partial\Delta H/\partial t$). For data collected in 1.0 mM $MgCl_2$, the fit excluded data

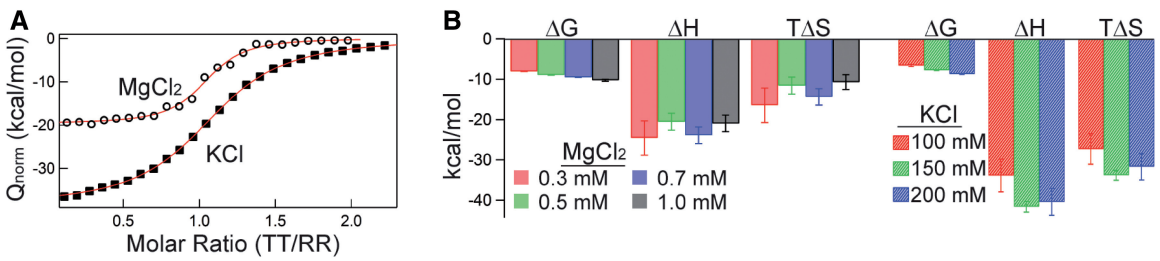

Figure 3. Thermodynamics of TT–RR binding in $MgCl_2$ and KCl solutions. (**A**) Representative titration comparison in conditions eliciting comparable complex stabilities. Open circles, 0.5 mM $MgCl_2$, 20°C, titrant [TT] = 229 μM, starting cell [RR] = 10 μM. Solid squares, 150 mM KCl, 20°C, titrant [TT] = 145 μM, starting cell [RR] = 10 μM. (**B**) Left, linear fit-determined maximum likelihood ΔG_{25C}, ΔH_{25C} and $T\Delta S_{25C}$ in 0.3 (red), 0.5 (green), 0.7 (blue) and 1.0 mM (black) $MgCl_2$. Right, ΔG_{25C}, ΔH_{25C} and $T\Delta S_{25C}$ in 100 (red), 150 (green) and 200 (blue) mM KCl.

Table 1. Thermodynamic and kinetic parameters for TT–RR binding in Mg^{2+}

Temp. (°C)	K_a (M^{-1}) × 10^5	ΔG°_{obs} (kcal/mol)	ΔH°_{obs} (kcal/mol)	$T\Delta S^\circ_{obs}$ (kcal/mol)	k_{on} ($M^{-1}s^{-1}$)	k_{off} (s^{-1}) × 10^{-5}
0.3 mM $MgCl_2$						
10	–[a]	–[a]	−20.5 (±3.3)	–[a]	200 (±80)	3.2 (±1.3)
20	18 (±5)	−8.4 (±0.4)	−21.9 (±5.0)	−13.6 (±5.2)	270 (±60)	13 (±10)
30	5.6 (±1.3)	−8.0 (±0.3)	−26.9 (±4.2)	−19.0 (±4.0)	510 (±210)	87 (±13)
0.5 mM $MgCl_2$						
2	–	–	−20.7 (±4.1)	–	310 (±180)	0.4 (±0.5)
5	–	–	−19.6 (±2.1)	–	420 (±60)	1.0 (±0.1)
10	–	–	−17.8 (±2.7)	–	600 (±140)	3.3 (±0.7)
15	–	–	−19.6 (±3.9)	–	630 (±410)	6.4 (±6.2)
20	64 (±7)	−9.1 (±0.2)	−18.9 (±2.0)	−9.8 (±2.0)	940 (±80)	16 (±4)
30	24 (±1)	−8.9 (±0.1)	−23.2 (±1.9)	−14.3 (±1.9)	1530 (±120)	62 (±7)
0.7 mM $MgCl_2$						
10	–	–	−20.5 (±3.0)	–	1240 (±30)	1.7 (±0.1)
20	160 (± 4)	−9.7 (±0.1)	−24.8 (±3.2)	−15.1 (±3.2)	2360 (±60)	14 (±1)
30	56 (± 2)	−9.4 (±0.1)	−22.4 (±3.1)	−13.1 (±3.1)	3130 (±550)	58 (±8)
1.0 mM $MgCl_2$						
5	–	–	−19.4 (±3.0)	–	1690 (±270)	0.7 (±0.1)
10	–	–	−18.4 (±2.2)	–	2230 (±210)	2.2 (±0.2)
15	–	–	−18.9 (±3.7)	–	3180 (±630)	6.7 (±1.3)
20	–	–	−19.5 (±2.3)	–	3950 (±540)	15 (±2)
25	–	–	−23.6 (±4.7)	–	5660 (±4890)	57 (±42)
30	–	–	−21.3 (±2.1)	–	5800 (±580)	68 (±6)
35	55 (±7)	−9.5 (±0.2)	−23.9 (±3.0)	−14.3 (±3.1)	6810 (±1510)	120 (±20)
40	23 (±5)	−9.1 (±0.3)	−26.7 (±3.7)	−17.5 (±3.8)	7840 (±2060)	310 (±50)
45	9.9 (±2.1)	−8.7 (±0.3)	−28.6 (±5.5)	−19.9 (±5.8)	–	–

– not determined because ITC c-value greater than 200
–[a] not determined because post-injection decay too slow to accurately integrate throughout titration

Table 2. Thermodynamic and kinetic parameters for TT–RR binding in K^+

Temp. (°C)	K_a (M^{-1}) × 10^5	ΔG°_{obs} (kcal/mol)	ΔH°_{obs} (kcal/mol)	$T\Delta S^\circ_{obs}$ (kcal/mol)	k_{on} ($M^{-1}s^{-1}$)	k_{off} (s^{-1}) × 10^{-5}
100 mM KCl						
5	52 (±3)	−8.5 (±0.1)	−35.1 (±3.8)	−26.6 (±3.8)	550 (±60)	10 (±1)
15	5.9 (±0.7)	−7.6 (±0.2)	−34.9 (±2.8)	−27.3 (±2.8)	530 (±90)	95 (±14)
150 mM KCl						
5	–	–	−39.4 (±1.5)	–	2290 (±200)	3.9 (±0.3)
10	–	–	−38.7 (±1.6)	–	2250 (±80)	12 (±1)
15	58 (±4)	−8.9 (±0.1)	−40.4 (±2.6)	−31.5 (±2.6)	2300 (±70)	38 (±8)
20	18 (±1)	−8.4 (±0.1)	−40.6 (±1.7)	−32.2 (±1.8)	2200 (±60)	110 (±20)
25	4.7 (±0.2)	−7.7 (±0.1)	−41.8 (±1.9)	−34.1 (±1.9)	2190 (±90)	440 (±30)
200 mM KCl						
5	–	–	−37.9 (±5.2)	–	6080 (±200)	3.2 (±0.3)
10	–	–	−37.1 (±3.3)	–	6060 (±460)	9.5 (±0.7)
20	76 (±3)	−9.2 (±0.1)	−40.0 (±4.2)	−30.8 (±4.1)	5680 (±1040)	76 (±16)
25	27 (±5)	−8.8 (±0.2)	−46.3 (±4.8)	−37.4 (±4.8)	6170 (±370)	180 (±50)
30	9.4 (±6.9)	−8.3 (±0.1)	−43.9 (±4.2)	−35.7 (±4.3)	5810 (±650)	650 (±90)

– not determined because ITC c-value greater than 200.

above 30°C, where the binding enthalpy displays a statistically significant change in slope (Supplementary Figure S2). This observation corroborates our previous hypothesis that the free receptor exists in a temperature-dependent conformation (32). In other words, the enthalpy becomes increasingly temperature dependent at temperatures where the melting intermediate becomes significantly populated. While the shift in ΔC_p may begin between 20 and 30°C (Tables 1 and 2, Supplementary Figure S2), overall the ΔC_p is small and negative for the full set of experiments conducted below 30°C. The average ΔC_p below 30°C are similar in $MgCl_2$ and KCl solutions: bootstrap analysis yields −0.14 (±0.02) kcal/mol/K in $MgCl_2$ versus −0.04 (±0.08) kcal/mol/K in KCl. The weighted average ΔC_p for a single tetraloop–receptor interaction is therefore −0.06 (±0.02) kcal/mol/K. This value is not far from that predicted by a coarse-grained surface area burial calculation (−0.002 kcal/mol/K) (39).

The free energy at 25°C (ΔG_{25C}) in Table 3 is also a maximum likelihood value (interpolated in 5 of the 7 salt conditions) determined from K_a ($\Delta G^\circ = -RT\ln K_a$) according to its temperature dependence using the van't Hoff equation.

$$\frac{\partial \ln K_a}{\partial 1/T} = -\frac{\Delta H_{VH}}{R} \quad (5)$$

Table 3. Average Thermodynamic parameters

Salt	Temp (°C)	ΔG_{25C} (kcal/mol)	ΔH_{25C} (kcal/mol)	$T\Delta S_{25C}$ (kcal/mol)	ΔC_p (kcal/mol/K)	ΔH_{VH} (kcal/mol)
0.3 mM $MgCl_2$	10–30	−8.1 (±0.1)	−24.6 (±4.3)	−16.5 (±4.4)	−0.21 (±0.15)	−24.2 (±0.6)
0.5 mM $MgCl_2$	2–30	−9.0 (±0.1)	−20.5 (±2.1)	−11.6 (±2.1)	−0.12 (±0.10)	−17.4 (±2.9)
0.7 mM $MgCl_2$	10–30	−9.5 (±0.1)	−23.9 (±2.0)	−14.4 (±2.0)	−0.17 (±0.06)	−17.8 (±1.0)
1.0 mM $MgCl_2$	5–45	−10.2 (±0.2)	−20.9 (±2.1)	−10.7 (±2.3)	−0.11 (±0.05) −0.57 (±0.29)[a]	−31.0 (±6.7)[a]
100 mM KCl	5–15	−6.6 (±0.3)	−34.0 (±4.1)	−27.4 (±4.5)	0.11 (±0.31)	−36.4 (±3.8)
150 mM KCl	5–25	−7.8 (±0.1)	−41.6 (±1.3)	−33.8 (±1.4)	−0.13 (±0.07)	−42.4 (±2.5)
200 mM KCl	5–30	−8.8 (±0.1)	−40.4 (±3.3)	−31.7 (±3.3)	−0.16 (±0.10)	−37.6 (±3.5)

[a]Determined from 30–45°C; all other values determined using temperatures ≤30°C.

The van't Hoff enthalpies (ΔH_{VH}) determined from Equation (5) agree well with the ΔH_{25C} values (Table 3). Only in 1.0 mM $MgCl_2$ is there a noticeable discrepancy between ΔH_{25C} and ΔH_{VH}, because K_a measurements in 1.0 mM $MgCl_2$ were performed across the temperature range 30–45°C, where ΔH is significantly more exothermic than it is from 10 to 30°C. The overall strong agreement shown in Table 3 corroborates homogeneous, one-to-one binding and underscores the robustness of van't Hoff equation-based extrapolations of K_a for kinetics analysis (below).

The 25°C entropy contribution ($T\Delta S_{25C}$) in Table 3 was calculated according to the Gibbs equation using ΔG_{25C} and ΔH_{25C}. $T\Delta S_{25C}$ is large and negative in all cases, indicating an unfavorable contribution. Parameter uncertainty and the relatively small number of salt concentrations examined in this study do not allow an unambiguous determination of whether the [salt]-dependence of the stability is largely entropically or enthalpically based, but additional data show it to be largely entropic as expected (16,40,41) (Supplementary Figure S3).

Comparison of the kinetics of tetraloop–receptor association in KCl and $MgCl_2$

Representative kinetic analyses of the titrations in Figures 2 and 3 are displayed in Figure 4. Figure 4A plots the deconvolved power trace and respective fitted curves for injections 2, 7 and 12 from the representative titration collected in 0.5 mM $MgCl_2$, 20°C, and a similar sampling of peaks and fits from the 150 mM KCl, 20°C dataset is displayed in Panel B. The resulting forward rate constants, k_{on}, are plotted for each injection from the first half of each titration (all injections such that $[TT]_{total} > [RR]_{total}$) in Figure 4C. As is visible in the raw data (Figure 2A), the observed rate of association decreases appreciably with each subsequent injection over the course of the first half of the titration, reflecting the decreasing concentration of unbound RR. Because k_{on} is a microscopic rate constant, it is independent of the RNA concentration (Figure 4C); the weighted-average k_{on} for these experiments are 860 (±50) $M^{-1}s^{-1}$ in $MgCl_2$ and 2180 (±240) $M^{-1}s^{-1}$ in KCl. The faster association of TT–RR in KCl versus $MgCl_2$ solution at ambient temperatures and respective salt concentrations eliciting similar stabilities is consistent with extant RNA folding literature (22–24).

The bimolecular kinetics equation applied to obtain k_{on} requires knowledge of K_a ('Materials and Methods' section). For many conditions in this work, the binding strength is in an optimal window, so K_a can be obtained with high precision and the measured value can be directly inserted into the kinetic analysis. However, in many of the low temperature experiments, the binding constant is greater than $2 \times 10^7\,M^{-1}$ (i.e. $c > 200$), so in these cases K_a was determined by van't Hoff extrapolation. Note that for these roughly stoichiometric binding scenarios, error in K_a only weakly influences k_{on} ('Materials and Methods' section). k_{off} was subsequently calculated according to the assumption of a single step mechanism, i.e. $k_{off} = k_{on}/K_a$. k_{on} and k_{off} measurements for all conditions are listed alongside the aforementioned thermodynamic results in Tables 1 and 2. The rate constants observed in this work are consistent with those obtained by Downey *et al.* (19), using a tethered tetraloop–receptor construct (Supplementary Data).

Analysis of the temperature dependence of k_{on} and k_{off} using the Eyring equation allows a thermodynamic characterization of the transition state.

$$\ln(k) = \ln(\alpha) + \frac{\Delta S^{\ddagger}}{R} - \frac{\Delta H^{\ddagger}}{RT} \quad (6)$$

The slope in a plot of $\ln(k)$ against the inverse temperature reveals the transition state enthalpy ($\Delta H^{\ddagger}$) in the slope and a term containing the transition state entropy ($\Delta S^{\ddagger}$) in the y-intercept. The so-called pre-exponential term (α) (42) is necessary to recover $\Delta S^{\ddagger}$ and has been discussed in the context of RNA folding elsewhere (43,44); here we simply assume a value within the range of possible values for macromolecular folding (43–46), as our intention is merely to provide $\Delta S^{\ddagger}$ values for comparison among salt conditions. Because turnover probability is a fundamental property of the transition state, it is almost certainly not influenced by salt type or concentration, thus application of a single α-value to all conditions is the only requirement for rigorous comparative analysis. Additionally, the logarithmic relationship between $\Delta S^{\ddagger}$ and α means the likely maximum error in $T\Delta S^{\ddagger}$ is no more than a few kcal/mol.

Figure 5 plots the logarithms of k_{on} and k_{off} against inverse temperature for all of the experiments in this work. In $MgCl_2$ (Figure 5A), the slopes ($-\Delta H^{\ddagger}/R$) for each salt concentration and both reaction directions are

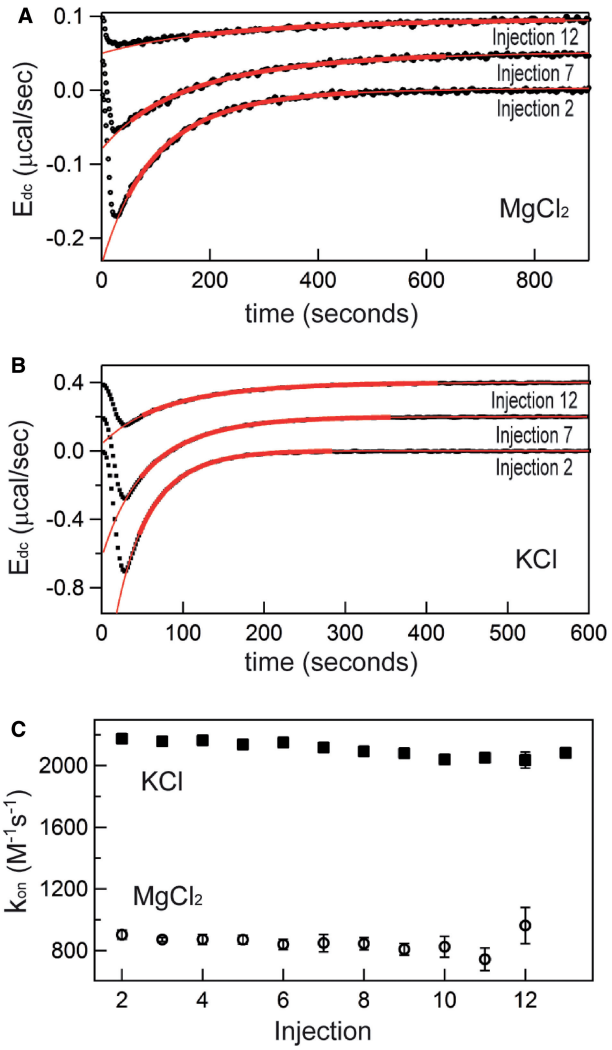

Figure 4. Representative kinetics (k_{on}) measurements from titrations in either 0.5 mM $MgCl_2$ or 150 mM KCl at 20°C (titrations are the same as those in Figures 2 and 3). (**A**) Selected deconvolved energies (E_{dc}) and fits for peaks 2, 7 and 12 for titration performed in 0.5 mM $MgCl_2$, 20°C. Bold red lines represent target function description of the data using best-fit parameters over the time range used in fitting; extrapolations of these functions are displayed in thin red lines. Peaks 7 and 12 are arbitrarily offset from 0 to aid visualization. (**B**) Representative peaks and fit functions for titration in 150 mM KCl, 20°C. (**C**) Corresponding complete population of k_{on} values from sampled titrations. Solid squares, KCl data; Open circles, $MgCl_2$ data.

negative, indicating that $\Delta H^{\ddagger}$ is large and positive for both association and dissociation. The full set of transition state theory thermodynamic quantities are listed in Table 4. $\Delta H^{\ddagger}_{on}$ is on average 8.1 (±0.5) kcal/mol in $MgCl_2$ solutions. This is consistent with a previous measurement, which used an oligonucleotide linker to monitor intra-construct tetraloop–receptor association via FRET, and determined an upper limit $\Delta H^{\ddagger}_{on}$ of 12.7 kcal/mol in 10 mM $MgCl_2$ (19). Using the aforementioned α-value, the average entropy contribution to forming the transition state ($T\Delta S^{\ddagger}_{on}$) from the unbound starting state is small and slightly favorable: 2.4 (±0.5) kcal/mol. For dissociation (k_{off}), the slopes are significantly steeper than the association plots, indicating even larger values for $\Delta H^{\ddagger}_{off}$. The difference in association and dissociation transition state enthalpies is consistent with the binding exothermicity (Table 3). Also notable in Figure 5A is the difference between the [$MgCl_2$]-dependence of the association and dissociation profiles. In plots of k_{on} there exists a significant and systematic trend in the rate constants measured at a common temperature, manifested as a horizontal offset. However, for k_{off} the temperature-dependent plots are nearly collinear. This behavior reflects a much more significant [$MgCl_2$]-dependence in k_{on} than in k_{off}.

Eyring plots obtained in KCl are displayed in Figure 5B. The data bear a strong resemblance to $MgCl_2$ data with one particularly striking difference: the temperature-dependence of k_{on} is almost entirely absent and is in fact slightly in the opposite direction as the $MgCl_2$ data for all KCl solutions, indicating that $\Delta H^{\ddagger}_{on}$ is slightly negative. Thus, the cation identity-based difference in $\Delta H^{\ddagger}_{on}$ parallels the observed difference in ΔH for the equilibrium binding process (Figure 3 and Table 3). The average $\Delta H^{\ddagger}_{on}$ value in KCl is −0.5 (±0.3) kcal/mol in KCl, a slightly favorable contribution that is much less than the unfavorable average value of 8.1 (±0.5) in $MgCl_2$. $T\Delta S^{\ddagger}_{on}$ is similarly reduced in KCl to an unfavorable average value of −5.9 (±0.3) kcal/mol, contrasting with the transition state entropy term in $MgCl_2$.

Trends in the salt concentration dependence of binding and rate constants are listed in Table 5, according to the log–log slope, using the molal salt activity (a_{salt}) as the dependent variable. These dependences report the change in the salt preferential interaction coefficient ($\Delta\Gamma_{salt}$) for a process (16,34), which conveys the net cation uptake into the RNA coulombic atmosphere. The salt activity dependence for the equilibrium binding event, $\partial \ln K_a/\partial \ln(a_{salt})$ is 6.2 (±0.5) in KCl and 2.8 (±0.1) in $MgCl_2$. This approximately 2-fold difference is consistent with the cation valences.

In $MgCl_2$, the [salt]-dependence of the binding constant is almost entirely explained through the on-rate. The dependence of k_{on} ($\partial \ln k_{on}/\partial \ln(a_{MgCl2})$) accounts for most of the dependence of K_a on a_{MgCl2}, whereas the off-rate exhibits a negligible a_{MgCl2}-dependence (Table 5). In KCl the situation is slightly more balanced: the k_{on} a_{KCl}-dependence is 61% as large as $\partial \ln K_a/\partial \ln(a_{KCl})$, while the relative magnitude of the reverse rate constant quantity is approximately half as large.

DISCUSSION

TT–RR association in the context of RNA folding

As generally observed for RNA folding, tetraloop–receptor driven helical packing exhibits highly salt-dependent behavior (20,47,48) and is enthalpy-driven (2,4,49–55). The results here demonstrate that the exothermicity can be extremely solution dependent, with the association enthalpy varying by as much as 20 kcal/mol. Additional data indicate that it is the balance of Mg^{2+} and K^{+} concentrations that is most relevant to the thermodynamic structure of the folding landscape (17) (Supplementary Figures S4 and S5). Mikulecky *et al.* (54) also observed a significantly less

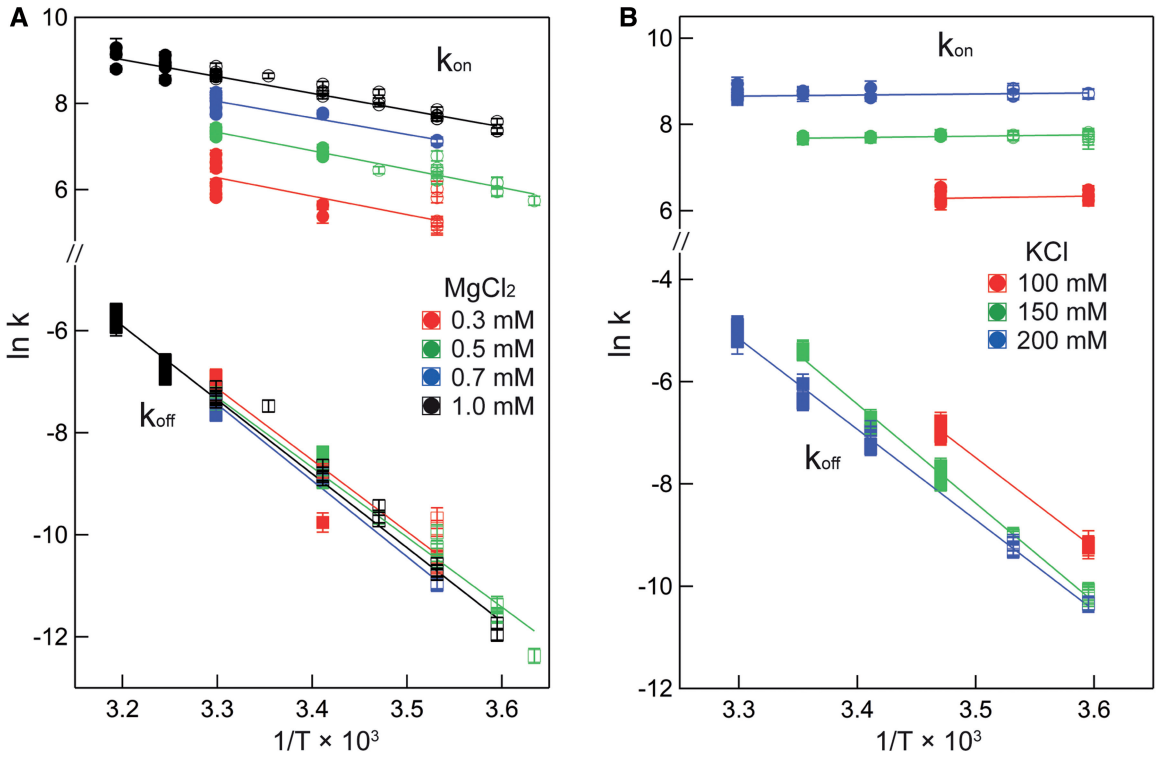

Figure 5. Eyring plot of both association (k_{on}) and dissociation (k_{off}) rate constants measured in $MgCl_2$ and KCl solutions. Each symbol represents the average rate constant measurement from a single titration, and error bars represent the measurement's true uncertainty as described in Supplementary Material. Circles, k_{on}; squares, k_{off}. For both rate constants, closed symbols reflect data that were obtained from titrations where K_a was measured directly ($1 \times 10^5\,M^{-1} < Ka < 2 \times 10^7\,M^{-1}$), while for open symbols, $K_a > 2 \times 10^7\,M^{-1}$. Lines were generated using best-fit regression parameters. (**A**) $MgCl_2$ data, (**B**) KCl data. Y- and X-axis scaling are identical in the two panels.

Table 4. Average kinetic parameters

Salt	Temp (°C)	$k_{on,25C}$ ($M^{-1}s^{-1}$)	$\Delta H^{\ddagger}_{on}$ (kcal/mol)	$^{a}T\Delta S^{\ddagger}_{on,25C}$ (kcal/mol)	$k_{off,25C}$ (s^{-1})	$\Delta H^{\ddagger}_{off}$ (kcal/mol)	$^{a}T\Delta S^{\ddagger}_{off,25C}$ (kcal/mol)
0.3 mM $MgCl_2$	10–30	380 (±140)	6.3 (±1.4)	−0.5 (±1.5)	$3.3\ (\pm 1.8) \times 10^{-4}$	25.8 (±6.0)	10.7 (±6.4)
0.5 mM $MgCl_2$	2–30	1160 (±100)	7.3 (±2.4)	1.2 (±2.4)	$3.3\ (\pm 0.6) \times 10^{-4}$	26.9 (±2.4)	11.9 (±2.5)
0.7 mM $MgCl_2$	10–30	2770 (±140)	8.7 (±0.7)	3.1 (±0.7)	$2.8\ (\pm 0.3) \times 10^{-4}$	30.3 (±1.7)	15.1 (±1.9)
1.0 mM $MgCl_2$	5–40	4840 (±630)	7.8 (±1.1)	2.5 (±1.1)	$3.1\ (\pm 0.5) \times 10^{-4}$	28.8 (±1.8)	13.8 (±1.8)
100 mM KCl	5–15	510 (±100)	−1.0 (±1.4)	−7.5 (±1.5)	$7.6\ (\pm 2.0) \times 10^{-3}$	35.4 (±2.3)	22.3 (±2.4)
150 mM KCl	5–25	2200 (±50)	−0.4 (±0.6)	−6.2 (±0.6)	$3.9\ (\pm 0.5) \times 10^{-3}$	38.6 (±1.1)	25.0 (±1.2)
200 mM KCl	5–30	5770 (±270)	−0.5 (±0.4)	−5.6 (±0.4)	$2.2\ (\pm 0.2) \times 10^{-3}$	35.3 (±1.4)	21.5 (±1.5)

[a]Determined using pre-exponential term $\alpha = 1 \times 10^{10}\ s^{-1}$ (for comparison, application of $\alpha = 6 \times 10^{12}\ s^{-1}$ would decrease all $T\Delta S^{\ddagger}$ by ~3.8 kcal/mol).

Table 5. Salt activity dependence decomposition, $\Delta\Gamma_{salt}$

Salt	$\frac{\partial \ln K_a}{\partial \ln(a_{salt})}$	$\frac{\partial \ln k_{on}}{\partial \ln(a_{salt})}$	$\frac{\partial \ln k_{off}}{\partial \ln(a_{salt})}$
$MgCl_2$	2.8 (±0.1)	2.2 (±0.2)	−0.1 (±0.3)
KCl	6.2 (±0.5)	3.8 (±0.2)	−2.0 (±0.4)

negative enthalpy for folding the hammerhead ribozyme in a solution containing added $MgCl_2$, with a $\Delta\Delta H$ of 24 kcal/mol in solutions containing 100 mM NaCl and either 0 or 10 mM $MgCl_2$.

Kinetic studies of RNA folding have generally observed a (large) positive activation enthalpy (3–5,44,47,56–63), and these studies were almost all conducted in solutions containing millimolar concentrations of $MgCl_2$. Interestingly though, Cole and Crothers (3) identified a tRNA tertiary structure transition with $\Delta H^{\ddagger}$ ~0 kcal/mol for formation in a solution lacking $MgCl_2$ (4). Here we observe a large positive $\Delta H^{\ddagger}_{on}$ in $MgCl_2$ solutions but a lower, near-zero enthalpic barrier in KCl solutions. The tRNA result and the [$MgCl_2$]-dependent hammerhead ribozyme ΔH suggests potential generality to these findings.

Figure 6 summarizes the thermodynamic reaction coordinate profiles for TT–RR binding in solutions containing either $MgCl_2$ or KCl, using representative conditions (0.5 mM $MgCl_2$ or 150 mM KCl). A sizeable enthalpic

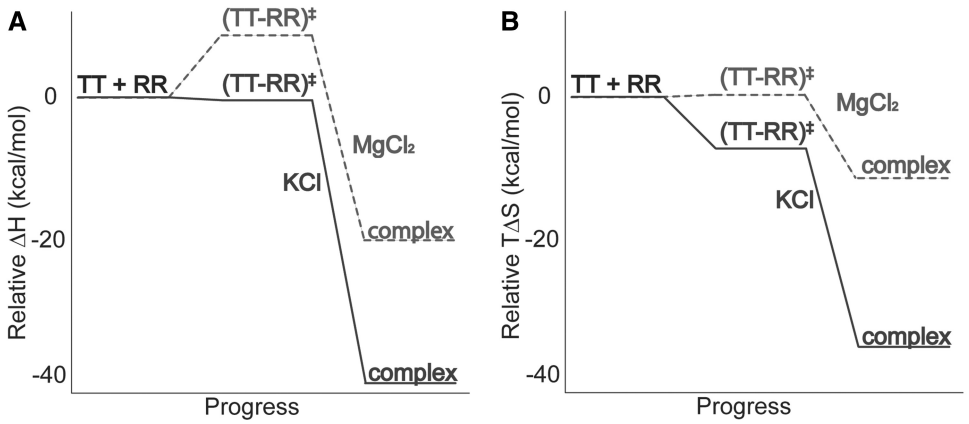

Figure 6. (**A**) Enthalpic (ΔH) and (**B**) entropic ($T\Delta S$) contributions to the free energy of TT–RR association in KCl (solid line) and $MgCl_2$ (dashed line) solutions, relative to the starting state. The schemes represent values in 150 mM KCl or 0.5 mM $MgCl_2$ at 25°C.

barrier to association in $MgCl_2$ of 7.3 kcal/mol contrasts with the slightly negative $\Delta H^{\ddagger}_{on}$ of −0.6 kcal/mol in KCl (Figure 6A). The overall binding process is 21.7 kcal/mol more exothermic in KCl. Thus both steps in the reaction, formation of the transition state from the unbound state and conversion to the bound state from the transition state, are more favorable enthalpically in KCl than in $MgCl_2$ (by 7.9 and 13.8 kcal/mol, respectively). The entropic contribution to binding ($T\Delta S$) is essentially the reverse energetically of the enthalpic diagram (Figure 6B). In other words, formation of the transition state and subsequent conversion to the bound state are each more entropically opposed in KCl than in $MgCl_2$. The reason for the stepwise disparity cannot be resolved from our data; it may relate to the bivalent construct design if the folding pathway traverses two similar activation barriers on the way to the final bound state.

The data suggest that the transition state is relatively compact; in other words, the transition state is at least a partially associated TT–RR complex. In both $MgCl_2$ and KCl, the forward rate constant [salt]-dependence, $\partial \ln k_{on}/\partial \ln(a_{salt})$ constitutes most of the a_{salt}-dependence of the overall association process, $\partial \ln K_a/\partial \ln(a_{salt})$ (Table 5). This result is in line with the analogous process of double helix formation (64), and suggests the charge density of the rate-limiting transition state is most similar to that of the final bound state. The [salt]-dependence breakdown for TT–RR is also similar to that previously identified by Nesbitt and co-workers using a tethered tetraloop–receptor design. They found $\partial \ln k_{on}/\partial \ln[MgCl_2] = 0.49$ to be approximately 2/3 of the overall $\partial \ln K_a/\partial \ln[MgCl_2] = 0.74$ (65). This agreement suggests that a compact transition state is not specific to the bimolecular design in our study.

While the evidence points to a compact transition state, it may not involve tertiary contacts. Previous investigations of RNA folding identified an 'early' transition state; i.e. a state lacking specific stabilizing tertiary contacts (43,44,66). Bokinsky *et al.* (66) went on to also characterize the [salt]-dependence of hairpin ribozyme folding. As is true here for tetraloop–receptor mediated helical packing, the [salt]-dependence of hairpin ribozyme folding is almost entirely in the forward direction in $MgCl_2$. Moreover, in the monovalent salt NaCl, the hairpin ribozyme [salt]-dependence is more balanced between the forward and reverse rate constants, further paralleling our TT–RR association data. Bokinsky *et al.* concluded that the transition state is compact yet early, and further hypothesized that in monovalent salt, the transition state may be slightly less compact than in $MgCl_2$. This interpretation is consistent with the data herein for tetraloop–receptor mediated helical packing.

Potential explanations for cation-dependent ΔH and $\Delta H^{\ddagger}$

We consider two conceptual explanations for the cation-dependent TT–RR binding profile highlighted by Figure 6. Either there is a cation-dependent difference in the RNA structure that influences the thermodynamics of folding, or the explanation lies in the difference in the thermodynamics of potassium and magnesium ion uptake that occurs concomitant with tetraloop–receptor association. The difference is not directly related to the potassium 'binding' site (28,34,67) (Supplementary Table S2 and Figure S6). In the discussion below we focus on the cation-dependence in enthalpy terms because entropy terms are strongly [salt]-dependent, whereas ΔH is only weakly [salt]-dependent in these physiological salt concentration regimes (16,40) (Supplementary Figure S3).

In terms of structural explanations, we think the most likely interpretation invokes a salt-dependent unbound receptor conformation. For example, if a free receptor conformation such as that previously observed (68) were stabilized by magnesium, the unbound state would be enthalpically stabilized and a corresponding penalty for obligate disruption of this structure would be observed in forming the transition state and final bound state in $MgCl_2$, but not in KCl. There is some precedence for this functional behavior as kinetic traps in large RNA folding are more prevalent in solutions containing Mg^{2+} and little or no monovalent salt (22,48,57). The effect here does not appear to be related to a structural effect induced by some level of 'ionic strength', however (Supplementary Figure S4).

Alternatively and potentially of more generality, cation hydration may explain the divergent thermodynamic

profiles in KCl and $MgCl_2$. Formation of the transition or bound state from the unbound state requires an uptake of cations due to the increased charge density (Table 5). Thus it may be that the uptake of diffuse monovalent and divalent cations by the tetraloop–receptor contact in particular, or in folded RNA structures in general, occurs with different thermodynamic signatures. Most simply, partial dehydration of one or more Mg^{2+} accumulated in the local domain of the RNA might incur an additional enthalpic penalty concomitant with formation of both the transition state and final bound state. Given a Mg^{2+} dehydration enthalpy of ~450 kcal/mol, even a slight disturbance in an outer hydration shell could explain this difference (69).

We favor this ion hydration hypothesis because it is consistent with an early but compact transition state. There is evidence that Mg^{2+} accumulation by nucleic acids is accompanied by partial dehydration and is partially non-coulombic in nature (70,71), and replacement of sodium with magnesium in the local domain of polyU or polyA-polyU may be accompanied by a slightly positive ΔH (72). On the other hand, low-resolution data argue against a difference in ΔH for magnesium and monovalent cation accumulation near RNA (2,6).

The magnitude and generality of the phenomenon observed here may of course depend on RNA structural details. A slight variation on (or addition to) the ion hydration hypothesis focuses on differences in how cations affect RNA hydration. Magnesium, more than a monovalent cation, preferentially accumulates in the most electronegative regions of nucleic acids (9,73). Thus relative to K^+, complexation in the presence of Mg^{2+} is accompanied by a disproportionate release of RNA hydrating waters from these regions; if these water molecules possess a significantly favorable solvating enthalpy term, then their displacement will be observed as a positive ΔH contribution. Accumulation of Mg^{2+} may therefore displace a larger quantity of such highly enthalpically stabilized hydrating waters from the RNA than does K^+. As above this would yield the observed behavior that magnesium-driven RNA folding is associated with a larger enthalpic penalty.

Overall the data provide new insight into RNA folding in a physiological, mixed salt solution. Preliminary data suggest tertiary folding in physiological conditions may exhibit a balance of K^+ and Mg^{2+} stabilization (Supplemental Figure S5). One consequence of this finding would be that RNA folding *in vivo* does not exhibit the extreme temperature dependence in the rate of folding predicted by most *in vitro* studies, which have been conducted in solutions dominated by $MgCl_2$.

SUPPLEMENTARY DATA

Supplementary Data are available at NAR online.

ACKNOWLEDGEMENTS

We would like to thank Dr Julie Fiore, Dr Darrell McCaslin and the UW Biophysics Instrument Facility for helpful discussions and calorimeter maintenance. Thanks also to M. Thomas Record and Lauren Michael for manuscript comments. Data were obtained at the University of Wisconsin–Madison Biophysics Instrumentation Facility, which was established with support from the University of Wisconsin–Madison and grants BIR-9512577 (NSF) and S10 RR13790 (NIH). Kirk Vander Meulen performed the experiments, data analysis and manuscript preparation. Sam Butcher assisted in manuscript preparation and data analysis.

FUNDING

University of Wisconsin–Madison and (grants BIR-9512577) (NSF) and (S10 RR13790) (NIH); NSF (grant MCB-0445613 to S.E.B.). Funding for open access charge: University of Wisconsin, Madison Vilas Associate Award to S.E.B.

Conflict of interest statement. None declared.

REFERENCES

1. Chu,V.B. and Herschlag,D. (2008) Unwinding RNA's secrets: advances in the biology, physics, and modeling of complex RNAs. *Curr. Opin. Struc. Biol.*, **18**, 305–314.
2. Privalov,P.L. and Filimonov,V.V. (1978) Thermodynamic analysis of transfer-RNA unfolding. *J. Mol. Biol.*, **122**, 447–464.
3. Cole,P.E. and Crothers,D.M. (1972) Conformational changes of transfer ribonucleic acid. Relaxation kinetics of the early melting transition of methionine transfer ribonucleic acid (*Escherichia coli*). *Biochemistry*, **11**, 4368–4374.
4. Crothers,D.M., Cole,P.E., Hilbers,C.W. and Shulman,R.G. (1974) Molecular mechanism of thermal unfolding of *Escherichia-Coli* formylmethionine transfer-RNA. *J. Mol. Biol.*, **87**, 63–88.
5. Lynch,D.C. and Schimmel,P.R. (1974) Cooperative binding of magnesium to transfer ribonucleic-acid studied by a fluorescent-probe. *Biochemistry*, **13**, 1841–1852.
6. Rialdi,G., Biltonen,R. and Levy,J. (1972) Thermodynamic studies of transfer ribonucleic-acids .1. Magnesium binding to yeast phenylalanine transfer ribonucleic-acid. *Biochemistry*, **11**, 2472–2479.
7. Lindahl,T., Adams,A. and Fresco,J.R. (1966) Renaturation of transfer ribonucleic acids through site binding of magnesium. *Proc. Natl Acad. Sci. USA*, **55**, 941–948.
8. Stein,A. and Crothers,D.M. (1976) Conformational changes of transfer RNA. The role of magnesium(II). *Biochemistry*, **15**, 160–168.
9. Misra,V.K. and Draper,D.E. (2000) Mg2+ binding to tRNA revisited: the nonlinear Poisson–Boltzmann model. *J. Mol. Biol.*, **299**, 813–825.
10. Grilley,D., Soto,A.M. and Draper,D.E. (2006) Mg2+-RNA interaction free energies and their relationship to the folding of RNA tertiary structures. *Proc. Natl Acad. Sci. USA*, **103**, 14003–14008.
11. Misra,V.K. and Draper,D.E. (2001) A thermodynamic framework for Mg2+ binding to RNA. *Proc. Natl Acad. Sci. USA*, **98**, 12456–12461.
12. Soto,A.M., Misra,V. and Draper,D.E. (2007) Tertiary structure of an RNA pseudoknot is stabilized by "diffuse" Mg2+ ions. *Biochemistry*, **46**, 2973–2983.
13. Tan,Z.J. and Chen,S.J. (2010) Predicting ion binding properties for RNA tertiary structures. *Biophy. J.*, **99**, 1565–1576.
14. Bai,Y., Greenfeld,M., Travers,K.J., Chu,V.B., Lipfert,J., Doniach,S. and Herschlag,D. (2007) Quantitative and comprehensive decomposition of the ion atmosphere around nucleic acids. *J. Am. Chem. Soc.*, **129**, 14981–14988.

15. Kirmizialtin,S. and Elber,R. (2010) Computational exploration of mobile ion distributions around RNA duplex. *J. Phys. Chem. B*, **114**, 8207–8220.
16. Record,M.T., Zhang,W.T. and Anderson,C.F. (1998) Analysis of effects of salts and uncharged solutes on protein and nucleic acid equilibria and processes: A practical guide to recognizing and interpreting polyelectrolyte effects, Hofmeister effects, and osmotic effects of salts. *Adv. Protein Chem.*, **51**, 281–353.
17. Shiman,R. and Draper,D.E. (2000) Stabilization of RNA tertiary structure by monovalent cations. *J. Mol. Biol.*, **302**, 79–91.
18. Davis,J.H., Foster,T.R., Tonelli,M. and Butcher,S.E. (2007) Role of metal ions in the tetraloop-receptor complex as analyzed by NMR. *RNA*, **13**, 76–86.
19. Downey,C.D., Fiore,J.L., Stoddard,C.D., Hodak,J.H., Nesbitt,D.J. and Pardi,A. (2006) Metal ion dependence, thermodynamics, and kinetics for intramolecular docking of a GAAA tetraloop and receptor connected by a flexible linker. *Biochemistry*, **45**, 3664–3673.
20. Takamoto,K., He,Q., Morris,S., Chance,M.R. and Brenowitz,M. (2002) Monovalent cations mediate formation of native tertiary structure of the Tetrahymena thermophila ribozyme. *Nat. Struct. Biol.*, **9**, 928–933.
21. Uchida,T., He,Q., Ralston,C.Y., Brenowitz,M. and Chance,M.R. (2002) Linkage of monovalent and divalent ion binding in the folding of the P4-P6 domain of the Tetrahymena ribozyme. *Biochemistry*, **41**, 5799–5806.
22. Heilman-Miller,S.L., Pan,J., Thirumalai,D. and Woodson,S.A. (2001) Role of counterion condensation in folding of the Tetrahymena ribozyme II. Counterion-dependence of folding kinetics. *J. Mol. Biol.*, **309**, 57–68.
23. Shcherbakova,I., Gupta,S., Chance,M.R. and Brenowitz,M. (2004) Monovalent ion-mediated folding of the Tetrahymena thermophila ribozyme. *J. Mol. Biol.*, **342**, 1431–1442.
24. Sclavi,B., Sullivan,M., Chance,M.R., Brenowitz,M. and Woodson,S.A. (1998) RNA folding at millisecond intervals by synchrotron hydroxyl radical footprinting. *Science*, **279**, 1940–1943.
25. Laederach,A., Chan,J.M., Schwartzman,A., Willgohs,E. and Altman,R.B. (2007) Coplanar and coaxial orientations of RNA bases and helices. *RNA*, **13**, 643–650.
26. Costa,M. and Michel,F. (1995) Frequent use of the same tertiary motif by self-folding RNAs. *EMBO J.*, **14**, 1276–1285.
27. Toor,N., Keating,K.S., Taylor,S.D. and Pyle,A.M. (2008) Crystal structure of a self-spliced group II intron. *Science*, **320**, 77–82.
28. Cate,J.H., Gooding,A.R., Podell,E., Zhou,K.H., Golden,B.L., Kundrot,C.E., Cech,T.R. and Doudna,J.A. (1996) Crystal structure of a group I ribozyme domain: principles of RNA packing. *Science*, **273**, 1678–1685.
29. Tanner,M.A. and Cech,T.R. (1995) An important RNA tertiary interaction of group I and group II introns is implicated in gram-positive RNase P RNAs. *RNA*, **1**, 349–350.
30. Krasilnikov,A.S., Yang,X.J., Pan,T. and Mondragon,A. (2003) Crystal structure of the specificity domain of ribonuclease P. *Nature*, **421**, 760–764.
31. Jaeger,L., Westhof,E. and Leontis,N.B. (2001) TectoRNA: modular assembly units for the construction of RNA nano-objects. *Nucleic Acids Res.*, **29**, 455–463.
32. Vander Meulen,K.A., Davis,J.H., Foster,T.R., Record,M.T. Jr and Butcher,S.E. (2008) Thermodynamics and folding pathway of tetraloop receptor-mediated RNA helical packing. *J. Mol. Biol.*, **384**, 702–717.
33. Geary,C., Chworos,A. and Jaeger,L. (2011) Promoting RNA helical stacking via A-minor junctions. *Nucleic Acids Res.*, **39**, 1066–1080.
34. Lambert,D., Leipply,D., Shiman,R. and Draper,D.E. (2009) The influence of monovalent cation size on the stability of RNA tertiary structures. *J. Mol. Biol.*, **390**, 791–804.
35. Geary,C., Baudrey,S. and Jaeger,L. (2008) Comprehensive features of natural and in vitro selected GNRA tetraloop-binding receptors. *Nucleic Acids Res.*, **36**, 1138–1152.
36. Fiore,J.L., Kraemer,B., Koberling,F., Edmann,R. and Nesbitt,D.J. (2009) Enthalpy-driven RNA folding: single-molecule thermodynamics of tetraloop-receptor tertiary interaction. *Biochemistry*, **48**, 2550–2558.
37. Davis,J.H., Tonelli,M., Scott,L.G., Jaeger,L., Williamson,J.R. and Butcher,S.E. (2005) RNA helical packing in solution: NMR structure of a 30 kDa GAAA tetraloop-receptor complex. *J. Mol. Biol.*, **351**, 371–382.
38. Mayorga,O.L. and Freire,E. (1987) Dynamic analysis of differential scanning calorimetry data. *Biophys. Chem.*, **27**, 87–96.
39. Spolar,R.S., Ha,J.H. and Record,M.T. (1989) Hydrophobic effect in protein folding and other noncovalent processes involving proteins. *Proc. Natl Acad. Sci. USA*, **86**, 8382–8385.
40. Mascotti,D.P. and Lohman,T.M. (1993) Thermodynamics of single-stranded RNA and DNA interactions with oligolysines containing tryptophan - effects of base composition. *Biochemistry*, **32**, 10568–10579.
41. Vander Meulen,K.A., Saecker,R.M. and Record,M.T. (2008) Formation of a wrapped DNA-protein interface: Experimental characterization and analysis of the large contributions of ions and water to the thermodynamics of binding IHF to H ' DNA. *J. Mol. Biol.*, **377**, 9–27.
42. Kramers,H.A. (1940) Brownian motion in a field of force and the diffusion model of chemical reactions. *Physica*, **7**, 284–304.
43. Silverman,S.K. and Cech,T.R. (2001) An early transition state for folding of the P4-P6 RNA domain. *RNA*, **7**, 161–166.
44. Bartley,L.E., Zhuang,X., Das,R., Chu,S. and Herschlag,D. (2003) Exploration of the transition state for tertiary structure formation between an RNA helix and a large structured RNA. *J. Mol. Biol.*, **328**, 1011–1026.
45. Kubelka,J., Hofrichter,J. and Eaton,W.A. (2004) The protein folding 'speed limit'. *Curr. Opin. Struct. Biol.*, **14**, 76–88.
46. Dill,K.A. and Chan,H.S. (1997) From levinthal to pathways to funnels. *Nat. Struct. Biol.*, **4**, 10–19.
47. Silverman,S.K., Deras,M.L., Woodson,S.A., Scaringe,S.A. and Cech,T.R. (2000) Multiple folding pathways for the P4-P6 RNA domain. *Biochemistry*, **39**, 12465–12475.
48. Russell,R., Zhuang,X.W., Babcock,H.P., Millett,I.S., Doniach,S., Chu,S. and Herschlag,D. (2002) Exploring the folding landscape of a structured RNA. *Proc. Natl Acad. Sci. USA*, **99**, 155–160.
49. Gluick,T.C. and Draper,D.E. (1994) Thermodynamics of folding a pseudoknotted messenger-RNA fragment. *J. Mol. Biol.*, **241**, 246–262.
50. Laing,L.G. and Draper,D.E. (1994) Thermodynamics of RNA folding in a conserved ribosomal-RNA domain. *J. Mol. Biol.*, **237**, 560–576.
51. Fang,X.W., Golden,B.L., Littrell,K., Shelton,V., Thiyagarajan,P., Pan,T. and Sosnick,T.R. (2001) The thermodynamic origin of the stability of a thermophilic ribozyme. *Proc. Natl Acad. Sci. USA*, **98**, 4355–4360.
52. Klostermeier,D. and Millar,D.P. (2000) Helical junctions as determinants for RNA folding: Origin of tertiary structure stability of the hairpin ribozyme. *Biochemistry*, **39**, 12970–12978.
53. Banerjee,A.R., Jaeger,J.A. and Turner,D.H. (1993) Thermal unfolding of a group-I ribozyme - the low-temperature transition is primarily disruption of tertiary structure. *Biochemistry*, **32**, 153–163.
54. Mikulecky,P.J., Takach,J.C. and Feig,A.L. (2004) Entropy-driven folding of an RNA helical junction: An isothermal titration calorimetric analysis of the hammerhead ribozyme. *Biochemistry*, **43**, 5870–5881.
55. Szewczak,A.A., Podell,E.R., Bevilacqua,P.C. and Cech,T.R. (1998) Thermodynamic stability of the P4-P6 domain RNA tertiary structure measured by temperature gradient gel electrophoresis. *Biochemistry*, **37**, 11162–11170.
56. Fang,X.W., Pan,T. and Sosnick,T.R. (1999) Mg2+-dependent folding of a large ribozyme without kinetic traps. *Nat. Struct. Biol.*, **6**, 1091–1095.
57. Pan,T. and Sosnick,T.R. (1997) Intermediates and kinetic traps in the folding of a large ribozyme revealed by circular dichroism and UV absorbance spectroscopies and catalytic activity. *Nat. Struct. Biol.*, **4**, 931–938.
58. Zarrinkar,P.P. and Williamson,J.R. (1994) Kinetic intermediates in RNA folding. *Science*, **265**, 918–924.
59. Downs,W.D. and Cech,T.R. (1996) Kinetic pathway for folding of the tetrahymena ribozyme revealed by three UV-inducible crosslinks. *RNA*, **2**, 718–732.

60. Gluick,T.C., Gerstner,R.B. and Draper,D.E. (1997) Effects of Mg2+, K+, and H+ on an equilibrium between alternative conformations of an RNA pseudoknot. *J. Mol. Biol.*, **270**, 451–463.
61. Kao,T.H. and Crothers,D.M. (1980) A proton-coupled conformational switch of *Escherichia coli* 5S ribosomal RNA. *Proc. Natl Acad. Sci. USA*, **77**, 3360–3364.
62. Lang,K., Rieder,R. and Micura,R. (2007) Ligand-induced folding of the thiM TPP riboswitch investigated by a structure-based fluorescence spectroscopic approach. *Nucleic Acids Res.*, **35**, 5370–5378.
63. Wickiser,J.K., Cheah,M.T., Breaker,R.R. and Crothers,D.M. (2005) The kinetics of ligand binding by an adenine-sensing riboswitch. *Biochemistry*, **44**, 13404–13414.
64. Porschke,D., Uhlenbeck,O.C. and Martin,F.H. (1973) Thermodynamics and kinetics of helix-coil transition of oligomers containing GC base pairs. *Biopolymers*, **12**, 1313–1335.
65. Hodak,J.H., Downey,C.D., Fiore,J.L., Pardi,A. and Nesbitt,D.J. (2005) Docking kinetics and equilibrium of a GAAA tetraloop-receptor motif probed by single-molecule FRET. *Proc. Natl Acad. Sci. USA*, **102**, 10505–10510.
66. Bokinsky,G., Rueda,D., Misra,V.K., Rhodes,M.M., Gordus,A., Babcock,H.P., Walter,N.G. and Zhuang,X.W. (2003) Single-molecule transition-state analysis of RNA folding. *Proc. Natl Acad. Sci. USA*, **100**, 9302–9307.
67. Basu,S., Rambo,R.P., Strauss-Soukup,J., Cate,J.H., Ferre-D'Amare,A.R., Strobel,S.A. and Doudna,J.A. (1998) A specific monovalent metal ion integral to the AA platform of the RNA tetraloop receptor. *Nat. Struct. Biol.*, **5**, 986–992.
68. Butcher,S.E., Dieckmann,T. and Feigon,J. (1997) Solution structure of the conserved 16 S-like ribosomal RNA UGAA tetraloop. *J. Mol. Biol.*, **268**, 348–358.
69. Markham,G.D., Glusker,J.P. and Bock,C.W. (2002) The arrangement of first- and second-sphere water molecules in divalent magnesium complexes: results from molecular orbital and density functional theory and from structural crystallography. *J. Phys. Chem. B*, **106**, 5118–5134.
70. Kankia,B.I. and Marky,L.A. (1999) DNA, RNA, and DNA/RNA oligomer duplexes: A comparative study of their stability, heat, hydration, and Mg2+ binding properties. *J. Phys. Chem. B*, **103**, 8759–8767.
71. Paulsen,M.D., Anderson,C.F. and Record,M.T. (1988) Counterion exchange-reactions on DNA - Monte-Carlo and Poisson–Boltzmann analysis. *Biopolymers*, **27**, 1249–1265.
72. Krakauer,H. (1972) Calorimetric investigation of heats of binding of Mg++ to Poly a, to Poly U, and to their complexes. *Biopolymers*, **11**, 811–828.
73. Braunlin,W.H., Anderson,C.F. and Record,M.T. (1986) Na-23-Nmr investigations of counterion exchange-reactions of helical DNA. *Biopolymers*, **25**, 205–214.
74. Record,M.T. Jr, Anderson,C.F. and Lohman,T.M. (1978) Thermodynamic analysis of ion effects on the binding and conformational equilibria of proteins and nucleic acids: the roles of ion association or release, screening, and ion effects on water activity. *Q. Rev. Biophys.*, **11**, 103–178.